Mechanism of Ammonia Transport by Amt/MEP/Rh: Structure of AmtB at 1.35 Å

Shahram Khademi, Joseph O'Connell III, Jonathan Remis, Yaneth Robles-Colmenares, Larry J. W. Miercke, Robert M. Stroud*

The first structure of an ammonia channel from the Amt/MEP/Rh protein superfamily, determined to 1.35 angstrom resolution, shows it to be a channel that spans the membrane 11 times. Two structurally similar halves span the membrane with opposite polarity. Structures with and without ammonia or methyl ammonia show a vestibule that recruits NH_4^+/NH_3, a binding site for NH_4^+, and a 20 angstrom–long hydrophobic channel that lowers the NH_4^+ pK_a to below 6 and conducts NH_3. Favorable interactions for NH_3 are seen within the channel and use conserved histidines. Reconstitution of AmtB into vesicles shows that AmtB conducts uncharged NH_3.

The transport of ammonia/ammonium is fundamental to nitrogen metabolism throughout all domains of life (*1*–*4*). In what follows, Am refers to (NH_3 + NH_4^+), and MA to (CH_3NH_2+ $CH_3NH_3^+$). The so-called ammonia transporters (Amt proteins), whose paralogs in yeast are called methylammonium/ammonium permeases (MEP proteins) (*5*, *6*) are typically >420 amino acids in length and are assembled as trimers of proteins (*7*). The transport rates of most Amt/MEP proteins can be conveniently measured by transport of radioactive ^{14}C–labeled MA (*8*).

Plant, bacterial Amt, and yeast MEP family members show a range of concentration dependence for Am conductance up to "high affinity," as reflected in their ability to grow on very low concentrations (<5 μM) of ammonium salts as sole nitrogen source. The "response K_m" (the concentration that evokes half-maximal conductance) for Am is ~5 to 10 μM for MEP1 and 1 to 2 μM for MEP2. MEP3 is of much lower affinity, K_m ~ 2 mM (*6*). *amtB* and *glnK* located on the same operon, are cotranscribed in bacteria (*9*) and archaea, and GlnK plays a dynamic role in the regulation of nitrogen uptake (*10*) by binding to AmtB (*11*, *12*). In humans, the Rhesus (Rh) family of proteins, both erythroid (RhAG, RhD, and RhCE) and nonerythroid (RhCG, RhBG, and RhGK), also share conservation with the Amt/MEP family throughout their sequence (*13*) (Fig. 1).

Our structural analysis is based on crystals grown in the absence or presence of Am or MA. It reveals a recruitment vestibule for cations such as NH_4^+ or neutral NH_3, a site that can bind $CH_3NH_3^+$ or NH_4^+ using π-cation interactions, and a hydrophobic channel that incorporates NH_3 using weak interactions with C-H hydrogen bond donors. Our assays carried out on reconstituted vesicles show that the protein conducts NH_3 because addition of Am salts outside raises internal pH. This is therefore the first structure of a transmembrane channel family that can conduct unhydrated molecules that in isolation would be gaseous.

Department of Biochemistry and Biophysics, S412C Genentech Hall, University of California–San Francisco, 600 16th Street, San Francisco, CA 94143–2240, USA.

*To whom correspondence should be addressed. E-mail: stroud@msg.ucsf.edu

Structure Determination

We cloned two orthologs of AmtB, from *Aquifex aeolicus* (AmtB_AQFX) (*14*) and *Escherichia coli* (AmtB_*Ecoli*) (*4*, *7*). Twenty amino acids were excised from the N terminus of AmtB_AQFX and 22 were excised from AmtB_*Ecoli*, as established by matrix-assisted laser desorption/ionization mass spectroscopy (MALDI-MS) and N-terminal amino acid sequencing. This and the prediction of signal peptide cleavage sites through neural network approaches (*15*) led to the identification of these regions as signal sequences, which are removed upon insertion of the proteins into the cell membrane (Fig. 1). Crystals of AmtB_*Ecoli*, grown in the presence of 25 mM $AmSO_4$ at pH 6.5, diffract to a resolution of 1.35 Å (Table 1). Crystals of AmtB_AQFX diffracted to 4.5 Å and have not yet been pursued.

A Trimer of Three Channels

AmtB crystallizes as the physiological threefold symmetric trimer of channel-containing proteins (Fig. 2, A and B). The trimer extends ~65 Å parallel to the threefold axis and is 81 Å in diameter in the plane of the membrane. Eleven transmembrane-spanning α-helices (M1 to M11) form a right-handed helical bundle around each channel. Residues from M1, M6, M7, M8, and M9 of one monomer interact with helices M1, M2, and M3 of the neighboring monomer, with a total interacting surface area of 2716 $Å^2$. As described for other membrane proteins, polar aromatic side chains of residues Tyr^{62} at the periplasmic (termed extracellular) side and Tyr^{180}, Trp^{250}, and Trp^{297} at the cytoplasmic side would lie in the membrane-aqueous phase interface. The trimer has a net negative charge of –7.5 (13.5 positive + 21 negative) on the outer surface and a net positive charge of +9 (42

Table 1. Crystallographic statistics to 1.35 Å resolution. Crystals of SeMet AmtB (used for all crystallography) were in space group $P6_3$. Data were collected at the ALS beamline 8.3.1, with a CCD detector (Quantum 4), and integrated and scaled with DENZO, SCALEPACK (Native), and MOSFILM (MAD data). Phases were calculated with CCP4. After solvent flattening and phase extension to 2.0 Å, the model was refined with CNS to 1.8 Å and SHELX to 1.35 Å.

Data set	With 25 mM $AmSO_4$	With 100 mM $MASO_4$	Without Am/MA	SeMet MAD remote	SeMet MAD peak
Cell dimensions (*a* Å, *c* Å)	96.5, 94.6	95.7, 94.6	95.8, 94.7	95.8, 94.7	95.8, 94.7
Wavelength (Å)	1.1159	1.1159	1.1159	1.0080	0.9797
Resolution (Å)	1.35	1.85	2.0	2.5	2.5
Multiplicity	14.3	13.3	19.6	7.3	6.6
Completeness %*	97.3 (90.4)	99.7 (99.3)	87.4 (48.3)	99.7 (99.6)	99.7 (99.6)
I/σ	20.4 (1.6)	19.3 (1.9)	25.8 (2.0)	10.6 (3.3)	9.4 (2.8)
R_{sym} (%)	5.8 (62.1)	6.4 (80.0)	6.4 (69.5)	11.4 (81.0)	12.5 (87.0)
Phasing power				0.7	0.34
Figure of merit (after solvent flattening)				0.265 (0.877)	
R_{cryst}/R_{free} (%)	13.3/16.8	19.5/20.5	18.2/20.5		
RMSD bond length (Å)	0.007	0.007	0.013		
RMSD bond angle (°)	1.3	1.3	1.8		
Mean B factor ($Å^2$)	24.6	37.5	43.2		

*Numbers in parenthesis refer to the high-resolution shell for data refinement (1.45 to 1.40 with $AmSO_4$, 1.92 to 1.85 for $MASO_4$, and 2.07 to 2.00 for without substrate).

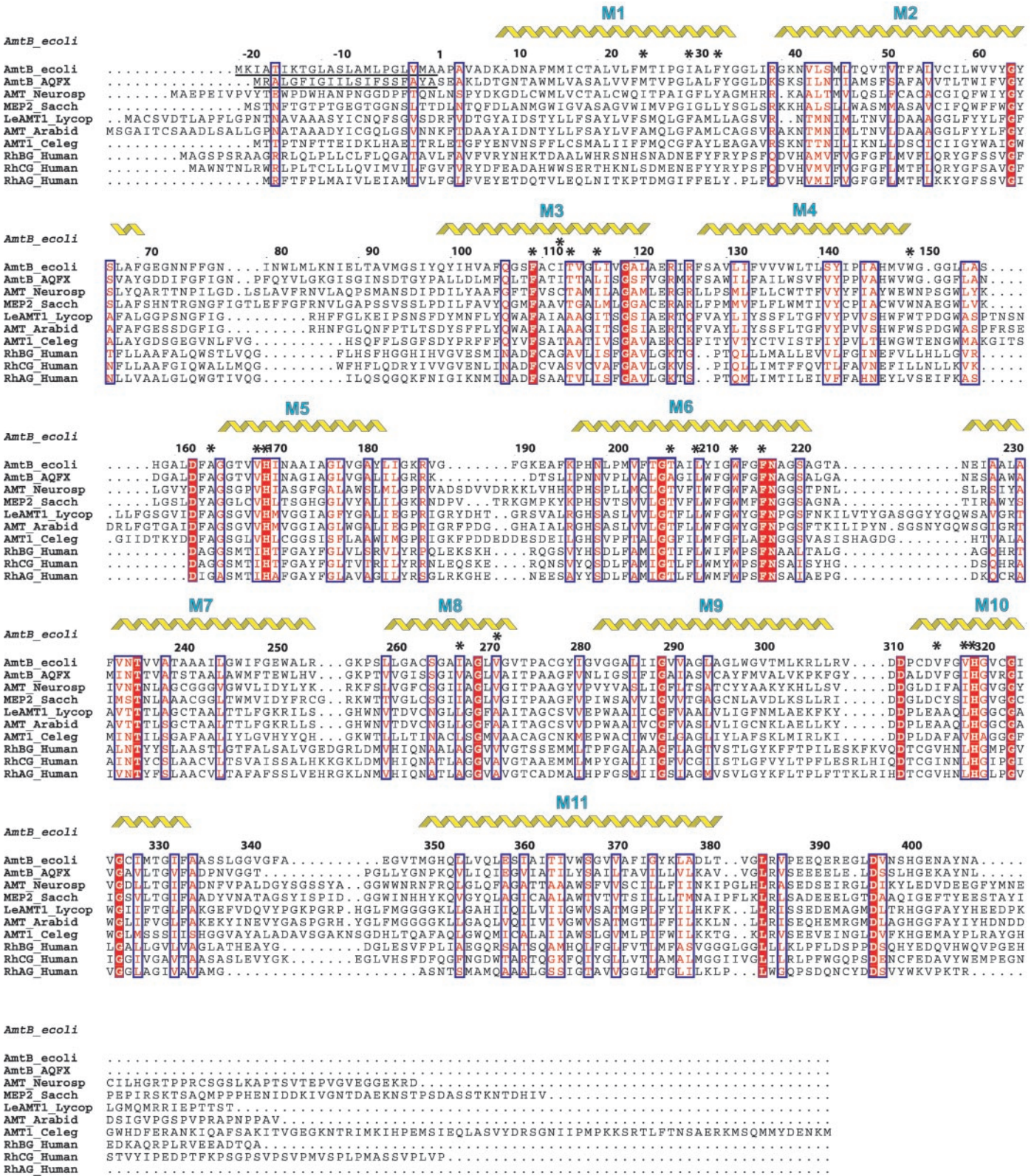

Fig. 1. The amino acid sequence alignments of AmtB/MEP/Rh homologs from *E. coli* (AmtB_*E. coli*), *A. aeolicus* (AmtB_AQFX), Neurospora (AMT_Neurosp), *Saccharomyces cerevisiae* (MEP2_Sacch), *Lycopersicon esculentum* (LeAMT1_Lycop), *Arabidopsis thaliana* (AMT_Arabid), *Caenorhabditis elegans* (AMT1_Celeg), and human Rh factors (RhBG, RhCG, and RhAG). The numbering is that of *E. coli* AmtB. Conserved amino acids are in white in red-filled rectangles. Similar residues are in red surrounded by blue lines. The signal sequences in *E. coli* and *A. aeolicus* are underlined. Residues that line the lumen of the channel are labeled with asterisks above. Eleven transmembrane helices are identified by helical motifs above the sequence, labeled by transmembrane helix numbers M1 to M11.

positive + 33 negative) on the cytoplasmic side, as is the trend in membrane proteins.

At the extracellular side, the threefold axis is surrounded by three closely packed copies of just M1 of each monomer, which seal the central axis against passage. Toward the cytoplasmic side, the three M1s (+16° to each other) veer away from the threefold axis to leave an open pocket ~10 Å across, formed by three copies of M1 and M6. M1 has a kink (22°) in the helix secured by the only cis-proline (Pro^{26}) in AmtB, a residue not conserved in the superfamily. M1 and M6 are not long enough to span the bilayer, consistent with the trimer being the stable physiological quaternary structure. The interfaces between subunits are almost as hydrophobic as the exterior, suggesting that a monomer could be transiently stable in the membrane upon synthesis, before forming trimers. An isolated square planar arrangement of four water molecules, each hydrogen-bonded to each other (average hydrogen bond length 3.0 Å), makes two hydrogen bonds to carbonyl oxygens of Cys^{56} and Ala^{102} in an otherwise hydrophobic cavity in the interface.

An 11-Crossing Membrane Protein with a Quasi-Twofold Axis in the Plane of the Membrane

We found that AmtB from *E. coli* and AmtB from *A. aeolicus* each begin with a signal sequence that is cleaved during synthesis. The topology of AmtB was correctly determined by a careful series of PhoA and LacZ insertions, and the C terminus was shown to be cytoplasmic (*4*). Within each AmtB channel, M1 to M10 diverge outward from the central plane in a right-handed helical bundle to generate a vestibule on each surface. Their inter helix angles are +26° to –58°. Within the trans-bilayer region, there are three glycine Cα-H. . .O=C hydrogen bonds (between the Cα hydrogen of glycine and a main chain carbonyl oxygen of a neighboring α-helix) between M1 and M6 (Gly^{204}, Gly^{211}, and Gly^{34}) and one between M8 and M10 (Gly^{325}). Cys^{109} and Cys^{56}, found only in *E. coli* AmtB, are close enough to form a disulfide in the transmembrane region.

The fold is not homologous to any other membrane protein structure previously reported. Although there is no evidence for any gene duplication in the family, the structure of M1 to M10 reflects a quasi-twofold axis in the midplane of the membrane that intersects the trimer threefold axis. It relates the structural context of the M1 to M5 region to that of M6 to M10. M11 is an additional ~50 Å–long straight helix, inclined at –50° to the perpendicular to the membrane plane that surrounds the lipid accessible side of each monomer (Fig. 2, B and C). This type of structural duplication with opposite polarity with respect to the membrane plane is seen in a number of membrane proteins, including AmtB, GlpF and all aquaporins, the SecY pro-

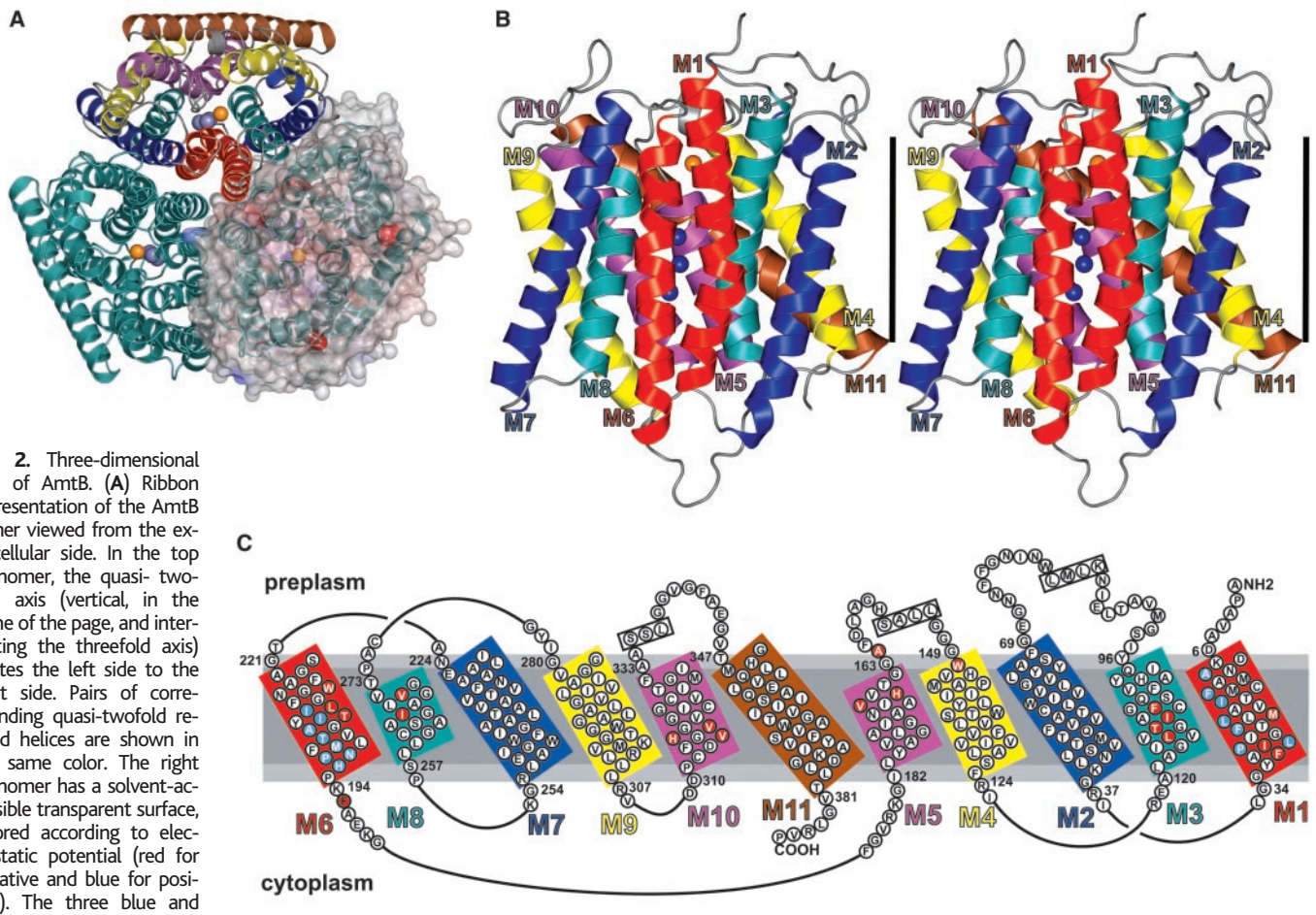

Fig. 2. Three-dimensional fold of AmtB. (**A**) Ribbon representation of the AmtB trimer viewed from the extracellular side. In the top monomer, the quasi- twofold axis (vertical, in the plane of the page, and intersecting the threefold axis) relates the left side to the right side. Pairs of corresponding quasi-twofold related helices are shown in the same color. The right monomer has a solvent-accessible transparent surface, colored according to electrostatic potential (red for negative and blue for positive). The three blue and one orange spheres are potential ammonia molecules and an ammonium ion, respectively. (**B**) A stereoview of the monomeric ammonia channel viewed down the quasi-twofold axis. In this and all subsequent figures, the extracellular side is uppermost. The vertical bar (35 Å) represents the inferred position of the hydrophobic portion of the bilayer. Three NH_3 molecules seen only when crystallized in the presence of ammonium sulfates, are shown as blue spheres. (**C**) The amino acid sequence of AmtB is arranged topologically as in the structure, with helices viewed as if from inside the channel looking away from the threefold axis. The quasi-twofold axis is perpendicular to the center of the figure. Five helices compose each segment, labeled M1 to M5 and M6 to M10. Related helices M1 and M6, M2 and M7, etc., are boxed in similar colors. Side chains of residues in red circles contribute to the substrate-contacting walls of the channel. Residues in blue circles contribute side chains to the inter-monomer contacts that immediately surround just the threefold axis of the trimer, because many oligomeric membrane proteins either need to insulate against passage of alternate molecules there or use this special location for stability, as in the aquaporins, or for conductance as in K^+ channels. The deduced location of the cell membrane is illustrated in gray (35 Å) with light gray for the head group region (to 40 Å thickness).

tein of the translocon, and the ClC chloride channel. However, of these, only in the aquaporin family were the vestiges of duplication recognized in the gene sequences (*16*). The sparse vestiges of duplication now apparent in sequence after the structure imply that they should be identifiable in other proteins when conservation among multiple sequences is taken into account. Because of the opposite polarity of the duplicated segments relative to the membrane, the primordial gene duplication event of such membrane proteins must have occurred before generation of enough functional surroundings to support any transport of molecules from one side of the membrane to the other.

The Mechanism of Transport or Conductance

We sought to define any preferred sites for Am or MA and the mechanism for transport or conductance of these molecules by comparison of the structure in the absence of any ammonium derivative, in 25 mM $AmSO_4$ at pH 6.5, and in 100 mM $MASO_4$ at pH 6.5. These concentrations are in ~1000-fold excess relative to the response K_m (Am, $K_m \sim 10$ μM; MA, $K_m \sim 50$ μM). There is no significant overall conformational change of the protein with Am or MA, consistent with AmtB as a channel rather than as an ammonia transporter that would harness alternating conformational states. Therefore, from now on, we refer to this family of molecules as channels.

The quasi-twofold (i.e., up to down) symmetric channel generated within each monomer by the structural antiparallel duplication begins with an extracellular vestibule. This is followed by one of two most constricted hydrophobic regions (Fig. 3A). The mid-membrane center of the pathway has two in-line histidines followed by the second constricted hydrophobic region and the intracellular vestibule. Between the two hydrophobic constrictions the channel wall is narrow and mostly nonpolar throughout its ~20 Å length, consistent with conduction of uncharged NH_3.

The outer vestibule contains 30 ordered water molecules. Am has similar density to that of H_2O; thus, if it replaces H_2O, it is difficult to identify unambiguously as Am. The density for MA is clearly distinguished from that of H_2O/Am, and the difference can uniquely mark a site. Because the Am and the MA crystals have slightly different unit cells and so were not isomorphous, Fo-Fo maps were not useful; thus, we cite Fo-Fc maps. One such MA site (60% ordered, where this order parameter represents the integrated electron content, referenced to the highest occupied water molecule) is located against both aromatic rings of Trp^{148} and Phe^{107} (Fig. 3B). The $-NH_3^+$ moiety is a hydrogen bond donor to the O_γ of Ser^{219}. This provides a favorable two π-cation interaction for NH_4^+ and for $CH_3NH_3^+$, stabilized by ring currents, and is accessible to solvent. MA displaces two separate peaks (Am1, 67% ordered) and a water peak in the Am structure (Fig. 3C), very similar to two water peaks in the H_2O structure (60% ordered). The order parameter we use primarily reflects movement in the site and secondarily statistical occupation.

Mutation of conserved Asp^{160} to Ala^{160} completely destroys transport of MA, implying that Asp^{160} plays a key role (*12*), and Merrick proposed that it might provide a primary binding site for NH_4^+. However, there is no peak of density against Asp^{160} even in the presence of 25 mM $AmSO_4$ or 100 mM $MASO_4$. Conserved Asp^{160} is a helix-capping residue for M5 (Fig. 4A), being a hydrogen bond acceptor at its Oδ2 from the Oγ H (2.51 Å) and N-H of Thr^{165} (2.8

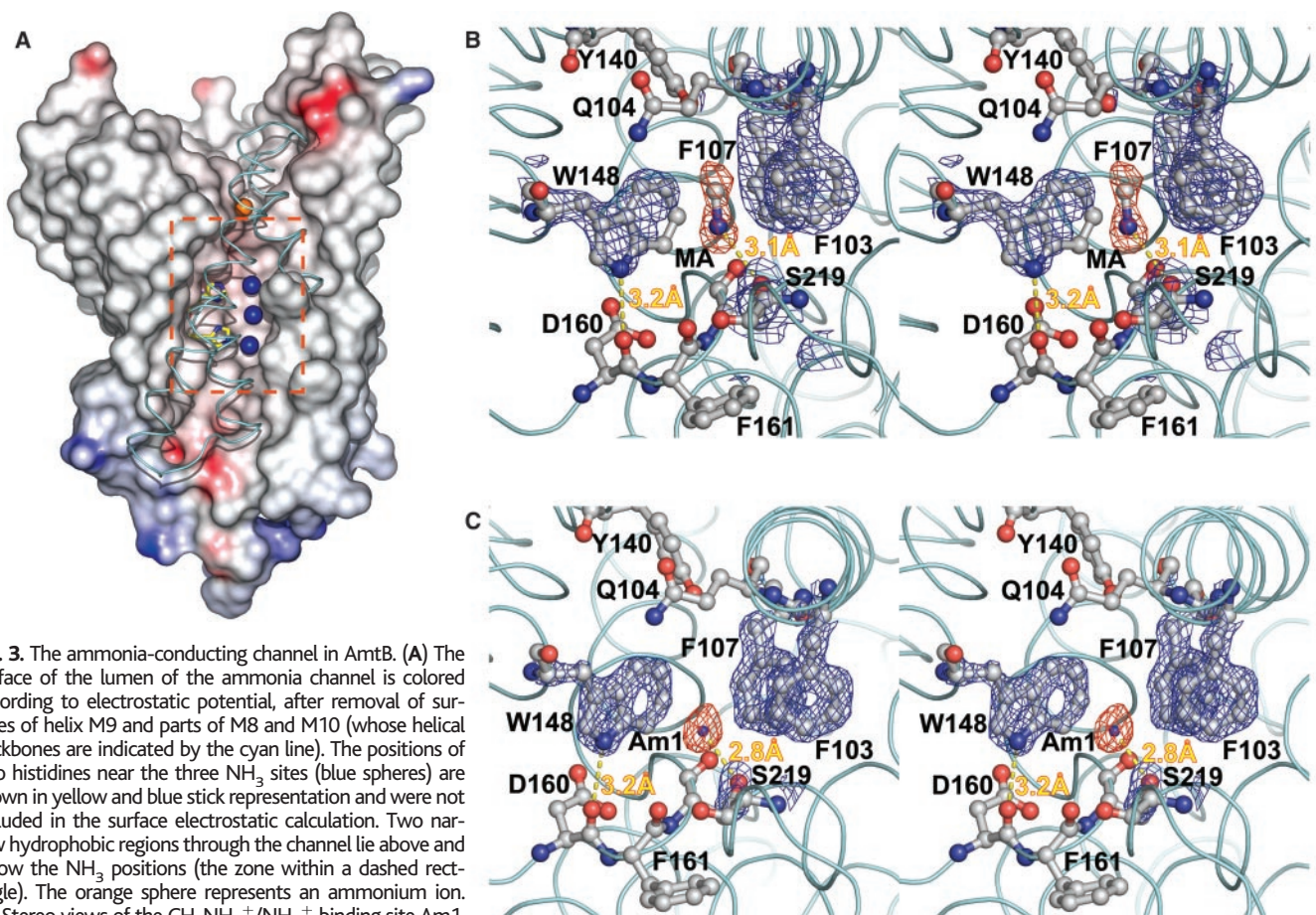

Fig. 3. The ammonia-conducting channel in AmtB. (**A**) The surface of the lumen of the ammonia channel is colored according to electrostatic potential, after removal of surfaces of helix M9 and parts of M8 and M10 (whose helical backbones are indicated by the cyan line). The positions of two histidines near the three NH_3 sites (blue spheres) are shown in yellow and blue stick representation and were not included in the surface electrostatic calculation. Two narrow hydrophobic regions through the channel lie above and below the NH_3 positions (the zone within a dashed rectangle). The orange sphere represents an ammonium ion. (**B**) Stereo views of the $CH_3NH_3^+/NH_4^+$ binding site Am1. The electron density map (2Fo-Fc) is contoured at 2σ for the protein (blue), and the (Fo-Fc) $CH_3NH_3^+$ omit map is contoured at 4.5σ (red) for AmtB in 100 mM $MASO_4$ at pH 6.5. The MA order is 67% occupancy for each (CH_3 and NH_3) group. Hydrogen bonds between the NH of $CH_3NH_3^+$ and Oγ of Ser^{219} and between the Nε1H of Trp^{148} and O of Asp^{160} are indicated by yellow dashed lines, with bond distance in yellow. (**C**) As in (B), for AmtB in 25 mM Am SO_4 at pH 6.5. Am order is 67% occupancy (6.7 electrons).

Å) and at its Oδ1 from the N-H of Gly^{164} (2.7 Å) and the N-H of Gly^{163} (2.8 Å) at the N-terminal end of M5. Thus, the Asp^{160} carboxyl orients the carbonyls of Asp^{160}, Phe^{161}, and Ala^{162} that, along with carbonyls of Ser^{68}, Ser^{219}, Val^{147}, and Trp^{148} from the outside ends of helices M2, M4, and M6, line the vestibule and make it cation-attracting. Asp^{160} itself is not accessible to bulk solvent and is conserved across the superfamily, underlying its key role that appears to be primarily structural. Cys^{326} shields one planar face of Asp^{160}. The indole ring of Trp^{148} is interposed between Asp^{160} and the MA site and shields Asp^{160} from solvent. Trp^{148} is conserved among the Amt/MEP subfamilies. The lowest polar carbonyl oxygen is for Ala^{162} at z = 8.5 Å. The first hydrophobic constriction in the channel formed by Trp^{148}, Phe^{103}, Phe^{161}, and Tyr^{140}, all of which are conserved only in Amt's, and everywhere conserved Phe^{107} and Phe^{215} suggests possible π-cation interactions for NH_4^+ on entry to the channel. The diameter is 1.2 Å; thus, the side chains of Phe^{107} and Phe^{215} must move dynamically during any conduction event.

In 25 mM $AmSO_4$, the crystal structure shows three additional peaks (Am2, Am3, and Am4 of order 20%, 15%, and 20%, respectively), not present without AmSO4 adjacent to two quasi-twofold, related, conserved imidazoles of His^{168} and His^{318} at the center of the narrow hydrophobic channel (Fig. 4, A and B). The partial order indicates that these Am-specific peaks are poorly ordered, consistent with there being no good localizing hydrogen bonds in the channel or with their being occupied alternately with each other, or conceivably partially occupied such that at higher concentration they might be fully occupied. This latter reason seems very unlikely, because Am is already at 1000-fold the K_m. At this resolution (1.35 Å), C, N, and O in AmtB are clearly distinguished. The orientation and hydrogen bonding of the imidazoles are unambiguously determined. The OH of conserved Thr^{273} is a hydrogen donor to the C=O of Leu^{269} and therefore an acceptor of the hydrogen bond from Nε2H of His^{168}. Unprotonated His^{168} Nδ1 and His^{318} Nδ1H are fixed by hydrogen bond to each other. They provide two Cε1-H hydrogen bond donors (*17*) to the N of Am2 and the N of Am3 (3.2 Å and 3.4 Å between heavy atoms, respectively), and one Nε acceptor for the N-H of Am4. The other surrounding side chains are all hydrophobic. π-cation stabilization is possible at Am2 from side chains of Phe^{215} and Trp^{212}. In this low dielectric environment, the imidazole Cε1-Hs will appear more acidic than imidazole in aqueous solution, because the effective dielectric constant (ε) is much lower. Therefore, coulombic attraction forces will increase as 1/ε.

Whereas imidazole nitrogens might act as a hydrogen donor N-H or an acceptor N at the lone pair of electrons on an unprotonated nitrogen, the Cε1–Hs can only be donors, easing passage of a molecule that is an acceptor, as is NH_3 but not NH_4^+. Thus, this signature structure harnesses all of its hydrogen-bonding potential to accommodate the passage of hydrogen bond–accepting molecules. The pK_a of NH_3 must be lowered to below 6 at sites Am3 and Am4, because peaks clearly reflect NH_3 at a pH of 6.5 in the crystals. At some point close to the aromatic constriction, NH_4^+ gives up its proton, leaving it predominantly on the side of entry, and NH_3 is transported. The cation-selective vestibule, possibly down to the Am2 site, can recruit NH_4^+. This and the aliphatic hydrophobic channel compatible with NH_3 can explain many of the seemingly inconsistent observations of function.

Phe^{31}, Tyr^{32}, and Val^{314} surround the second cytoplasmic constriction. Asp^{310}, the conserved quasi-twofold relative of Asp^{160}, similarly acts as a helix cap for M10. The first exit-peak of density within the channel pathway is hydrogen-bonded to Asp^{313} and could be close to where NH_3 would reacquire a proton on the inside to become NH_4^+.

Ammonia Conductivity by AmtB

In order to determine the substrate specificity and rates of conductance of AmtB, we adapted a fluorescence-based assay to measure the influx of ammonia into vesicles (liposomes or proteoliposomes) by monitoring the pH-sensitive fluorescence of 5-carboxy fluorescein (CF) (*18*, *19*). Rapid mixing of CF-loaded vesicles with ammonium chloride (0.5 mM or 5 mM) was initiated at pH 6.8. The internal pH rose, reflecting influx of NH_3 through the lipids and through AmtB, which subsequently acquires a proton from H_2O inside, to give NH_4^+ and OH^- (Fig. 5A).

The rate constant of ammonia influx indicated by the rate of pH change, 115.6 ± 13.2 s^{-1} (average of n = 6 determinations, typical curve fitting error in a single curve), for 5 mM NH_4Cl outside is 10-fold faster than for protein-free liposomes, 12.8 ± 0.7 s^{-1} (n = 6). The rate of pH change for 0.5 mM NH_4Cl (one tenth the concentration) is 70 s^{-1} (60% of the rate). Substitution of 5 mM NH_4Cl by 5 mM NaCl did not lead to any detectable change in fluorescence even after 10 s, showing that changes in CF fluorescence are due to ammonia influx and not, for example, to any water efflux due to change in osmolarity. As a further control, ammonia conductivity for proteoliposomes reconstituted with the aquaglyceroporin GlpF was measured at 11.4 ± 0.06 s^{-1} (n = 6), the same as for liposomes, consistent with there being no leakage due to the reconstitution procedure per se. Thus, when the ammonium concentration drops 10-fold, the rate drops only

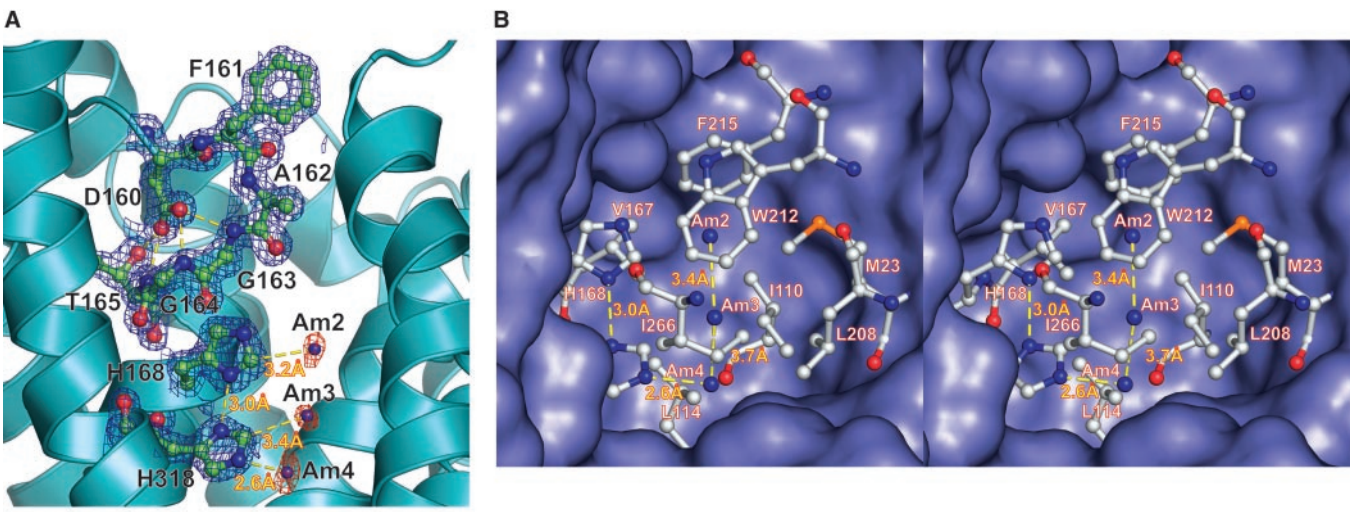

Fig. 4. (**A**) Electron density (2Fo-Fc) contoured at 1.5σ (blue) for the two-histidine region and surrounding structure, including conserved Asp^{160} that accepts four short hydrogen bonds (dashed yellow). Additional peaks Am2, Am3, and Am4 seen when crystallized with 25 mM ammonium sulfate are defined in the Fo-Fc omit map at 1.5σ (in red), indicating putative NH_3 molecule positions (blue spheres). The hydrogen-bonding network shows interactions between His^{168} and His^{318} and NH_3 peaks in yellow (distances in red). (**B**) Stereo view of the two-histidine center of the channel. Surrounding hydrophobic residues are shown in ball and stick representation. The surface representation covers other surrounding amino acids. Three ammonia-dependent sites are shown (blue spheres) with associated distances (dashed yellow line and yellow labels).

40%, generally consistent with the fact that the K_m for transport is below 500 μM Am.

To assess possible water conductivity by AmtB, osmotic permeability of water was measured by concentration-dependent self-quenching of vesicular CF with an aliquot of the same batch of AmtB proteoliposomes (*19*) (Fig. 5B), and also by light scattering as a monitor of vesicle shrinkage and swelling (*20*). By the fluorescence assay, when vesicles were mixed with sucrose to a final concentration of 250 mM sucrose outside, water efflux was 7.85 ± 0.08 s^{-1} ($n = 6$) for liposomes, versus 8.78 ± 0.07 s^{-1} ($n = 6$) for AmtB proteoliposomes, indicating no additional water conductivity in AmtB proteoliposomes, versus ~150 s^{-1} for a water channel AqpZ in the proteoliposomes. Thus, AmtB does not conduct water.

Likewise, the structure of AmtB without $(NH_4)_2SO_4$ showed no ordered water in between the hydrophobic constricted regions of the channel. Thus, the channel removes water of hydration from NH_4^+ and a proton, as NH_3 passes through the channel. The channel is narrow and the cost of dehydration of H_2O itself is not compensated by oxygen in the lumen of the channel, and no line of waters can be supported within the channel. This implication was also challenged by molecular mechanics simulation with NAMD, which after 2 ns of simulation confirmed that no water enters the channel (*21*).

The Mechanism: Recruitment of NH_4^+ and Filtered Passage of NH_3

The mechanism suggested by the atomic resolution structures, difference maps for Am/MA, and NH_3 conductivity in proteoliposomes involves a vestibular recruitment of total Am, a site that can bind NH_4^+, and a channel for NH_3 that lowers its pK_a to <6 (Fig. 6). This mechanism of conductance can reconcile many, but not yet, all data that lead to the seemingly inconsistent proposals of how members of the Amt/MEP family work.

Soupene *et al*. have maintained that the Amt/MEP family conducts NH_3 bidirectionally (*22*, *23*), with which our findings are consistent. On the basis of experiments, it has also been proposed that the Amt/MEP family variously transports NH_4+ (*9*, *24*–*26*), cotransport 26 and exchanges NH_3/H^+ (*26*), and exchanges NH_4^+/H^+ in Rh proteins (*27*, *28*). We attempt to address these data here.

pH-dependent effects. NH_4^+ (or $CH_3NH_3^+$) becomes less basic in the channel as it becomes progressively desolvated, until it reaches the Am2 position. At Am3, it is deprotonated and becomes uncharged (pK_a < 6). Entry of the uncharged NH_3 or CH_3NH_2 species into the hydrophobic channel at pHs above the new pK_a could eliminate all dependence of rate on pH and hence any dependence on concentration of the uncharged species in the bulk solution. Correspondingly, the solution equilibrium between NH_3 and NH_4^+ has little to do with the mechanism, because both species can enter the vestibule to become NH_3 at the Am2/3 site. If at all, lower pH might contribute to reduce the rate of Am conductance, not by reducing the level of NH_3 in bulk solution, but by opposing proton release from NH_4^+ in the vestibule. The vestibule may also have some preference for NH_4^+ or NH_3 that could be reflected as an indirect effect of pH in either direction; a tendency to recruit NH_4^+ would favor a small increase in rate at lower pH.

In *Coryne bacterium glutamicum*, two ammonia channels are present, Amt and AmtB. MA uptake has an apparent K_m ($CH_3NH_3^+$) of 53 ± 11 μM at pH 6.0 that is unchanged at pH 8.5, leading to the conclusion that NH_4^+ is the transported species, because NH_3 concentration in bulk solution would change 300-fold over this pH range, whereas NH_4^+ concentration is little changed (*25*, *29*). Likewise, the K_m for transport by *Arabidopsis* AMT2 is not pH-dependent between pH 5.0 and 7.5 (*30*). However, recruitment of Am to the vestibule can be completely pH-independent. Therefore, the inference that NH4$^+$ is conducted is incorrect; all Am will become NH_3 as it reaches the Am2/3 sites.

Effects of pH on transport of Am or MA by the human Rh factor RhAG show that the rate of inward transport of (external) $^{14}CH_3NH_3^+$ increases as external pH rises from 5.5 to 8.5 (*27*), tending to suggest that the neutral species may be conducted, because its concentration increases exponentially as pH is raised. However, a lack of effect of changes in membrane potential on conductance of MA, and a small decrease in conductance as internal pH rises, led to the conclusion that transport was electrically net neutral. Westhoff and colleagues reasoned that an increase in the outward-directed proton gradient might drive transport of ammonium ion, the predominant species in solution, and so suggested that RhAG might be a $H^+/CH_3NH_3^+$ antiporter. However, in light of our conclusions, it is of note that the increase in conductance was much more strongly dependent on the external pH than on internal pH, and it can equally be interpreted as transport of uncharged CH_3NH_2 as

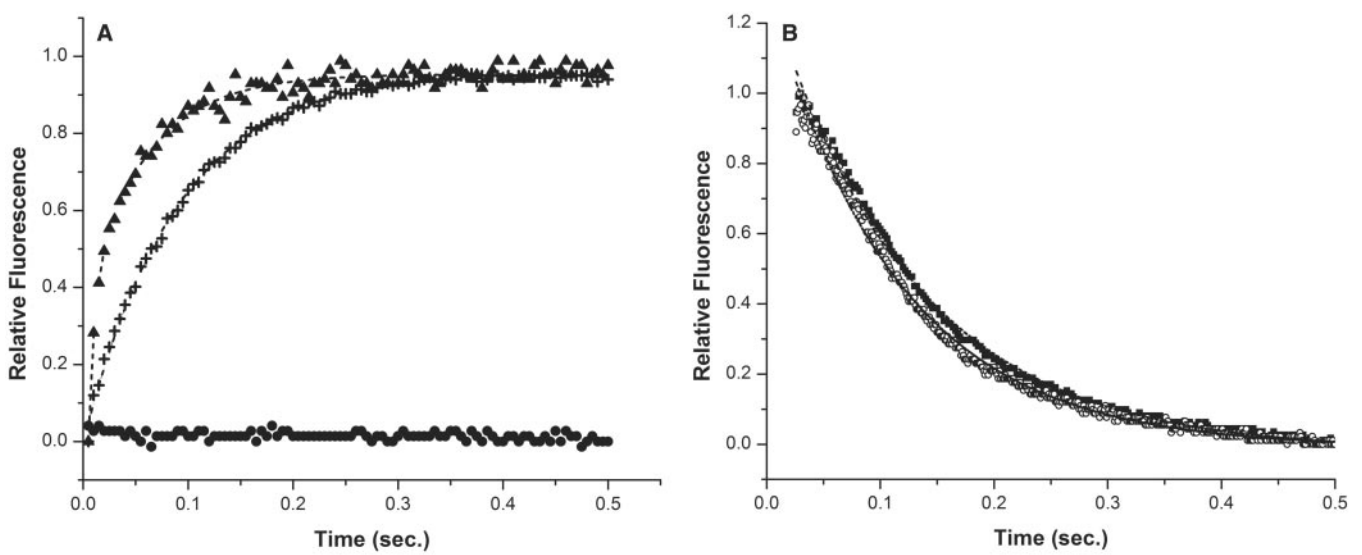

Fig. 5. Channel conductance in proteoliposomes. (**A**) The time course of change in pH inside of vesicles containing CF buffered by 20 mM Hepes as detected by fluorescence change. Initial pH was 6.8 both inside and outside. To initiate flux, 5 mM NH_4Cl was added externally to protein-free liposomes (+) and to AmtB-containing proteoliposomes (solid triangles) (protein to lipid ratio was 1:200 by weight) (*36*). To control for possible osmotic effects, instead of 5 mM NH_4Cl, 5 mM NaCl was added to proteoliposomes (solid circles). The dashed lines are exponential fits to the data. (**B**) Water conductance assessed by concentration-dependant self-quenching of CF-containing liposomes (solid squares) and proteoliposomes (open circles) upon addition of 500 mM sucrose at $t = 0$. The osmotic change leads to conductance of water through the lipids or through protein. The dashed lines are exponential fits to the data.

implied by our mechanism, in which the deprotonation of $CH_3NH_3^+$ in the vestibule might well become easier as pH is raised.

Soupene *et al*. show that growth in minimal nitrogen-limiting conditions of Am (≤1 mM) is especially deleterious at pH values below 7, where the effect of AmtB/MEP disruptions are profound (*22*). The bulk solution concentration of NH_3 decreases as pH is lowered, one reason that they propose that the Amt/MEP proteins increase the rate of equilibration of the uncharged species NH_3 across the membrane, rather than actively transporting the charged species NH_4^+ (*23*). Although our results are consistent with this conclusion, and with their findings that conductance is bidirectional, we contend that the effect of pH is not by effect on solution concentration of NH_3. Any pH dependence could be consistent with a possible pH effect on H^+ release from NH_4^+ in the vestibule. Consistent with this conclusion, the increase in rates of transport of MA versus pH do not increase by a factor of 10 per unit increase in pH as would be expected for a bulk pH effect, but increase by a factor of ~2 per pH unit (*27*).

Competitive inhibition. Ammonia channels conduct Am and MA but no larger secondary or tertiary amines. However, seemingly inconsistently, dimethylamine and ethylamine were found to inhibit the uptake of CH_3NH_2 by Amt and AmtB from *C. glutamicum*, whereas trimethyl- and tetramethyl amine did not (*25*). Although the channel is too small to accommodate these molecules, competition for the smaller cationic forms can take place at the Am1 site in the vestibule. This inhibition of MA conductance by Am in RhAG is pH-independent, surprisingly because their pK_as are different (*27*). However, we now would expect this pH independence because competition is between total MA and Am.

Transmembrane potential. Transmembrane potential accentuated conductance by the channel has been noted because K_m for MA decreases as transmembrane voltage (negative in the direction of conductance) increases, interpreted as indicating that NH_4^+ is conducted (*26*). However, the electric field will concentrate NH_4^+ on the NH_4^+ rich side of the membrane and in the vestibule, increasing the local concentration there and so explaining this effect. Thus, K_m (apparent) appears to be lower because the local concentration of MA/Am is higher in the vestibule than in the bulk solution.

Westhoff *et al*. show by expression of human RhAG in oocytes that the rate of conductance of MA remains constant even when membrane potential is modulated from –35 mV to –9 mV (inside the oocyte), concluding that transport is not electrogenic (*27*). This could be consistent with an electrically neutral NH_4^+/H^+ antiport mechanism as these authors suggest, but it is also consistent with net transport of uncharged CH_3NH_2 as our results imply.

All the observations noted so far are reconciled by the recruitment of NH_4^+, reduction of its pK_a and conductance of NH_3 as the primary mechanism. However, observations of ammonium-dependent currents through ammonia channels are not and demand further examination. A two-electrode voltage clamp was used to vary the transmembrane potential in oocytes transiently expressing the tomato paralog LeAMT1. Inward currents increased with voltage and with external ammonium ions from ~3 μM Am upward. The currents show a Hill coefficient of 1, implying that there is no cooperative effect of one conducted molecule of Am on another and suggesting a single binding site (*26*), which we presume could be Am1. This electrogenic behavior suggests that the channel transports ammonium ions (NH_4^+, or NH_3 plus a H^+) rather than uncharged NH_3. The measured currents are the same from pH 5.5 to 8.5 (*26*), consistent with conductance of NH_4^+ ions rather than with NH_3 and H^+, which might have showed some pH dependence. Although we have shown that AmtB conducts predominantly NH_3 (assayed in proteoliposomes), we have not shown that it does not conduct any occasional nonstoichiometric NH_4^+/H^+ ions that could give rise to these currents. A stoichiometric measure of conductance of each species NH_3/NH_4^+ will be required to establish whether this takes place at some low level. We do not see any hydrogen-bonded pathway that could act as a conductor for H^+, nor any change in conformation of AmtB determined in the presence of Am/MA. Given with these observations, one possibility is therefore that an occasional NH_4^+ ion can reach Am2, stabilized by ring currents of the rich aromatic environment at the constriction, and pass through the two-histidine region, possibly using the acid/base properties of the imidazole nitrogens to assist in proton transfer. This would require a transient conformational change that could be induced. The structure can clearly guide experimental measures of the ratio of conductances. Alternatively, the currents could be carried by another ion or another Am dependent pathway in the oocytes.

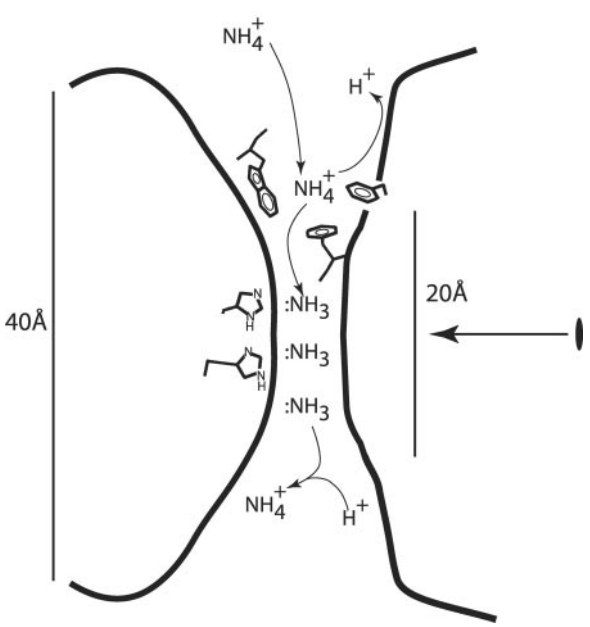

Fig. 6. The deduced mechanism of conductance is summarized. The low electron density for NH_3 may represent substitutional interchange or relative freedom of NH_3 within the hydrophobic channel. NH_3 normally undergoes rapid inversion. This may be impeded against the weak hydrogen bond C-H donors of imidazole.

The Mechanisms of Rh Factors

In light of the AmtB structure, the sequence of Rh factors can now be mapped onto the three dimensional structure of AmtB to address questions of Rh function. Variabilities in the Rh factors versus Amt/MEPs are seen in lengthened N- and C-terminal domains and in Rh-specific internal changes. The Rh proteins complement mutants in which all three of the yeast MEP proteins are inactivated (*mep1*Δ, *mep2*Δ, and *mep3*Δ), showing that the theRh proteins can provide similar function in the transport of Am to support the growth of yeast (*13*, *28*, *31*).

The rate of MA uptake in RhAG was saturable and well fitted by a Michaelis Menten equation with a K_m = 1.6 mM for the ionic species. NH_4^+ competed with MA (*27*). However, K_m for RhaG is 300-fold higher than for AtB and the Am1 site differs in lacking some of the π-cation stabilizing rings. Trp^{148} is Leu or Val in Rh factors; Phe/Tyr^{103} is Ile in Rh; Phe^{107} is conserved. This is consistent with low affinity for cations.

Based on several lines of evidence, Soupene *et al*. speculate that certain Rh factors, prominent in mammals and found alongside Amt in, for example, green algae, may function physiologically as channels for CO_2 (*32*, *33*). The stoichiometry of Rh factor associations in erythrocytes and their impact on the maternal immune response to fetal Rh are not known. Thus, the structure allows docking of models of the various Rh factors against each other to define this heterotrimeric assembly.

Biological Relevance of This Mechanism

Conductance of uncharged NH_3, versus NH_4^+ ion, can solve several biological problems. First, because K^+ channels conduct the very similarly sized NH_4^+ ion, there is the reverse possibility that an NH_4^+ ion channel could "leak" potassium and hence leak membrane potential in eukaryotes. Amt/MEP proteins are not permeable to any other ions (*26*). Transport of only uncharged NH_3 and not NH_4^+ assures this selectivity against all ions that would require replacement for their hydration shell while in the narrow portion of the channel. The energetic cost of removing even a single water of hydration from an ion is prohibitive. Second, NH_4^+ or any other ion is progressively energetically unstable as it approaches the center of the hydrophobic bilayer, whereas NH3 is much less so because it is electrically neutral. Potassium channels for example, have solved the problem by providing 16 carbonyl oxygens, 8 around each K^+ ion position on the way into the channel (*34*). Each oxygen offers a partial charge of 0.4 electrons to stabilize each K^+ ion. The KcsA channel also provides a water-filled cavity in the most energetically costly position at the center of the bilayer (*35*). The narrow hydrophobic channel of AmtB solves this energetic problem, as it also selects against the ionic form of NH_4^+ or any organic molecule larger in cross section than a single NH_3. Third, passage of uncharged NH_3 versus NH_4^+ would not leak proton motive force in conduction. Thus, neither energy nor any counter ion would be needed to accumulate ammonia.

Note added in proof: In a recent publication (*37*), it is shown that Am conductance by RhBG in oocytes is electroneutral, in contrast to the currents reported by the same group for another homolog (*26*), and can explain observations of electric currents in oocytes by an indirect mechanism. If general to the Amt/MEP/Rh family (Fig. 1), this would eliminate the only data that we discuss as potentially inconsistent with the mechanism we deduce.

References and Notes

1. J. Broach *et al.*, *J. Bacteriol.* **128**, 86 (1976).
2. M. A. Knepper *et al.*, *Physiol. Rev.* **69**, 179 (1989).
3. M. H. Saier Jr. *et al.*, *Biochim. Biophys. Acta* **1422**, 1 (1999).
4. G. H. Thomas *et al.*, *Mol. Microbiol.* **37**, 331 (2000).
5. A. M. Marini *et al.*, *EMBO J.* **13**, 3456 (1994).
6. A. M. Marini *et al.*, *Mol. Cell. Biol.* **17**, 4282 (1997).
7. D. Blakey *et al.*, *Biochem. J.* **364**, 527 (2002).
8. S. L. Hackette *et al.*, *J. Biol. Chem.* **245**, 4241 (1970).
9. R. Tate *et al.*, *Mol. Plant Microbe Interact.* **11**, 188 (1998).
10. M. R. Atkinson, A. J. Ninfa, *Mol. Microbiol.* **29**, 431 (1998).
11. G. Coutts *et al.*, *EMBO J.* **21**, 536 (2002).
12. A. Javelle *et al.*, *J. Biol. Chem.* **279**, 8530 (2004).
13. A. M. Marini *et al.*, *Trends Biochem. Sci.* **22**, 460 (1997).
14. E. Soupene *et al.*, *J. Bacteriol.* **184**, 3396 (2002).
15. H. Nielsen *et al.*, *Protein Eng.* **10**, 1 (1997).
16. J. H. Park, M. H. Saier Jr. *J. Membr. Biol.* **153**, 171 (1996).
17. Z. S. Derewenda *et al.*, *J. Mol. Biol.* **252**, 248 (1995).
18. A. Roos, W. F. Boron, *Physiol. Rev.* **61**, 296 (1981).
19. N. A. Priver *et al.*, *Biochemistry* **32**, 2459 (1993).
20. D. Fu *et al.*, *Science* **290**, 481 (2000).
21. S. Khademi *et al.*, unpublished data.
22. E. Soupene *et al.*, *Proc. Natl. Acad. Sci. U.S.A.* **95**, 7030 (1998).
23. E. Soupene *et al.*, *Proc. Natl. Acad. Sci. U.S.A.* **99**, 3926 (2002).
24. M. Y. Wang *et al.*, *Plant Physiol.* **103**, 1259 (1993).
25. J. Meier-Wagner *et al.*, *Microbiology* **147**, 135 (2001).
26. U. Ludewig *et al.*, *J. Biol. Chem.* **277**, 13548 (2002).
27. C. M. Westhoff *et al.*, *J. Biol. Chem.* **277**, 12499 (2002).
28. C. M. Westhoff *et al.*, *J. Biol. Chem.* **279**, 17443 (2004).
29. R. M. Siewe *et al.*, *J. Biol. Chem.* **271**, 5398 (1996).
30. C. Sohlenkamp *et al.*, *Plant Physiol.* **130**, 1788 (2002).
31. A. M. Marini *et al.*, *Nature Genet.* **26**, 341 (2000).
32. E. Soupene *et al.*, *Proc. Natl. Acad. Sci. U.S.A.* **99**, 7769 (2002).
33. E. Soupene *et al.*, *Proc. Natl. Acad. Sci. U.S.A.* **101**, 7787 (2004).
34. J. H. Morais-Cabral *et al.*, *Nature* **414**, 37 (2001).
35. Y. Jiang *et al.*, *Nature* **417**, 523 (2002).
36. Materials and methods are available as supporting material on *Science* Online.
37. U. Ludewig, *J. Physiol. (London)*, in press; published online 29 July 2004 (10.1113/jphysiol.2004.067728).

38. We thank J. Finer-Moore for her enlightened counsel, J. Holten for his assistance at the Advanced Light Source (ALS) beamline 8.3.1, and M. Mann for assistance in molecular biology. E. Soupene and S. Kustu suggested structure determination of an AmtB, and we thank them for providing an *Aquifex amtB* clone pJES1331, a solubilized cell pellet, and partially purified *Aquifex* protein. Supported by NIH grant no. GM24485 (R.M.S.). Coordinates (accession codes: apo, 1U77; Am, 1U7G; and MA, 1U7C) and structure factors (accession codes: apo, RCSB023331; Am, RCSB023340; and MA, RCSB023336) of the structures have been deposited in the Research Collaboratory for Structural Bioinformatics Protein Data Bank.

Supporting Online Material

www.sciencemag.org/cgi/content/full/305/5690/1587/DC1
Materials and Methods
References and Notes

24 June 2004; accepted 5 August 2004

REPORTS

Experimental Observation of Nonlinear Traveling Waves in Turbulent Pipe Flow

Björn Hof,[1]*† Casimir W. H. van Doorne,[1]* Jerry Westerweel,[1] Frans T. M. Nieuwstadt,[1] Holger Faisst,[2] Bruno Eckhardt,[2] Hakan Wedin,[3] Richard R. Kerswell,[3] Fabian Waleffe[4]

Transition to turbulence in pipe flow is one of the most fundamental and longest- standing problems in fluid dynamics. Stability theory suggests that the flow remains laminar for all flow rates, but in practice pipe flow becomes turbulent even at moderate speeds. This transition drastically affects the transport efficiency of mass, momentum, and heat. On the basis of the recent discovery of unstable traveling waves in computational studies of the Navier-Stokes equations and ideas from dynamical systems theory, a model for the transition process has been suggested. We report experimental observation of these traveling waves in pipe flow, confirming the proposed transition scenario and suggesting that the dynamics associated with these unstable states may indeed capture the nature of fluid turbulence.

Turbulence is one of the most common examples of complex and disordered dynamical behavior in nature. Typically, the motion of clouds, weather patterns, river flows, and even the flow from a faucet are turbulent. Yet the way in which turbulence arises and sustains itself is not understood even in laboratory experiments with well-controlled boundary conditions. The first study of this kind was undertaken by Reynolds (*1*) in 1883. He investigated the transition to turbulence in pipe flow and his observations have posed a riddle ever since. Whereas stability theory predicts that pipe flow will remain laminar for all flow rates (*2*), in practice pipe flow becomes turbulent even at moderate speeds. In contrast to other laminar-turbulence transitions, where primary and secondary instabilities of the laminar flow provide guidance, the transition process in pipe flow has remained a near total mystery. In pipes, turbulence sets in suddenly and fully, with no intermediate states and without a clear stability boundary.

Pipe flow can be described by a single dimensionless parameter, the Reynolds number $Re = UD/\nu$, where U is the mean (or bulk) flow speed, D the pipe diameter, and ν the kinematic viscosity of the fluid. In the laminar state, the flow profile is parabolic and the flow rate is proportional to the pressure